Electronic Supplementary Material (ESI) for Nanoscale.
This journal is © The Royal Society of Chemistry 2020

Supporting Information: Self-thermophoresis at the nanoscale using light induced solvation dynamics

Carles Calero,[†,§] Edwin L. Sibert III,[‡] and Rossend Rey[*,¶]

†*Departament de Física de la Matèria Condensada, Universitat de Barcelona, 08028 Barcelona, Spain*

‡*Department of Chemistry and Theoretical Chemistry Institute, University of Wisconsin-Madison, Madison, Wisconsin 53706, USA*

¶*Departament de Física, Universitat Politècnica de Catalunya, Campus Nord B4-B5, Barcelona 08034, Spain.*

§*Institut de Nanociència i Nanotecnologia, Universitat de Barcelona, Barcelona, Spain*

E-mail: rosendo.rey@upc.edu

Movie

MOVIE-Calero-Sibert-Rey.mp4: Trajectory of the Y-CNT-X molecule in the interior of the confining nanotube as its local dipoles Y-C and C-X are alternatively actuated. During the initial 1.4 ns of the trajectory only the C-X dipole (located on the right hand side of the Y-CNT-X molecule) is periodically inverted (with inversion period $\tau = 1$ ps). As a result, the molecule moves towards the left of the confining nanotube. During the second part of the trajectory, for times 1.4 n$s < t <$ 4.1 ns, the C-X dipole is not actuated and, instead, only the Y-C dipole is periodically switched (also with $\tau = 1$ ps). During this part of the

trajectory, the molecule travels in the opposite direction, that is towards the right of the confining nanotube. Finally, for the last part of the trajectory, i.e. for times 4.1 n$s < t <$ 6.1 ns, it is again only the C-X dipole which is actuated (still with $\tau = 1\,$ps), resulting in motion of the Y-CNT-X molecule towards the left of the confining nanotube as expected.

Simulation Details

The model for the C_{60}-X molecule considered in the main article consists of a C_{60} fullerene which is decorated with a single atom X, located at a distance 2.41 Å from carbon to which it is bonded (and along the direction defined by the bonded carbon and the center of mass of the C_{60} molecule, see Fig. 1a). We assign a charge q to the X moiety and $-q$ to the bonded carbon. The sign of q defines the direction of the localized dipole, which can be periodically switched with a characteristic period τ. The results reported in the main text correspond to $q = 1e$ and $\tau = 0.5, 1, 2, 5, 10\,$ps. In our simulations we have also considered smaller values for the charge ($q = 0.1e, 0.3e, 0.5e$), with qualitatively similar results.

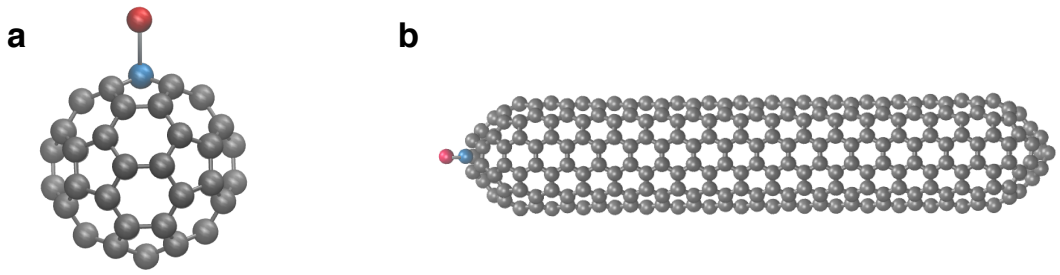

Figure 1: (a) model for C_{60}-X; (b) model for CNT-X.

The model for the CNT-X molecule consists of a 4 nm long (5,5)-carbon nanotube capped at its edges by 34 carbon atoms, and decorated with an atom X (see Fig. 1b). To generate the initial configuration of the capped-CNT we used the software *NanoCap*.[1,2] The functionalization with atom X is performed in a similar fashion as with the C_{60} molecule, although in this case the carbon atom to which X is bonded is the tip of the cap closing the (5,5)-CNT.

As in the previous case, X possesses a charge q and the bonded carbon a charge $-q$. In our simulations CNT-X is located in the interior of a 20 nm long (20,20)-CNT, generated with VMD.[3] During our simulations, the internal structure of the CNT-X molecule is maintained rigid and all the atoms of the confining (20,20)-CNT are kept in fixed positions.

Table 1: Parameters employed for the atomic Lennard-Jones interactions.

Atom	ϵ(kcal/mol)	σ (Å)
O	0.102	3.188
H	0.000	0.000
C (and X)	0.663	3.5811

For both cases considered (C_{60}-X in bulk water, and CNT-X in the interior of a (20,20)-CNT), the system is hydrated by water molecules ensuring that the mean density of water is $\rho \approx 1.0\,\mathrm{g/cm^3}$ (Fig. 2 displays the computed water density around C_{60}-X for the case of free diffusion). To avoid a significant global temperature drift of the solvent we have used systems containing a large number of water molecules. For C_{60}-X a cubic simulation box of side 20 nm containing $260,928$ water molecules has been used. For the simulations of CNT-X (and Y-CNT-X) we have used a square prism simulation box with sides $L_x = L_y = 10\,\mathrm{nm}$ and $L_z = 30\,\mathrm{nm}$, containing $93,414$ water molecules. For the solvent we have used the TIP3P-Ew model, a modified version of the three-point TIP3P model which improves the description of water properties and is suitable for simulations that use long-range electrostatic solvers, such as Ewald summation and particle-mesh-Ewald (PME).[5]

The non-bonded interactions between water molecules and the atoms of C_{60}-X, CNT-X, and the exterior (20,20)-CNT are described by electrostatic interactions and Lennard-Jones potentials with combination parameters given by the Lorentz-Berthelot combining rules. The Lennard-Jones parameters for oxygen and hydrogen atoms in water molecules, and the parameters for carbon and X atoms (taken identical) are given in Table 1. For all Lennard-Jones interactions, a cutoff of $r_c = 10$ Å is applied. Periodic boundary conditions are considered in the three spatial directions. To compute long-ranged electrostatic interactions the Ewald summation technique is employed. Time integration of the equations of motion

is performed using a velocity Verlet algorithm with a timestep $\Delta t = 1\,\mathrm{fs}$. All simulations are performed with the LAMMPS (31Mar2017 version) simulation package.[4]

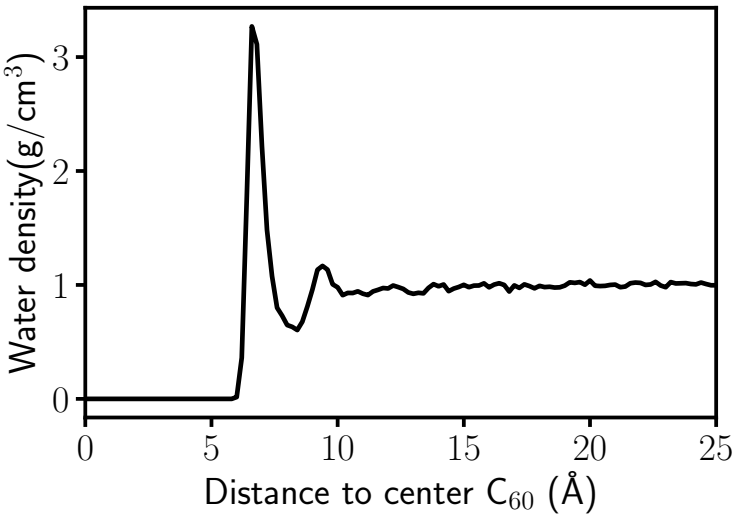

Figure 2: Density of water as a function of the distance to the center of C_{60}-X. Water bulk density is $\rho \approx 1.0\,\mathrm{g/cm^3}$. The first peak of water density is at a distance ≈ 6.6Å of the center of the C_{60}-X molecule.

In what concerns the equilibration protocol, after solvating the system we perform an energy minimization procedure by iteratively adjusting the coordinates of atoms to avoid undesired overlaps. Next, we run a short simulation (10,000 steps) in the NVT ensemble, employing a reduced timestep $\Delta t = 0.1\,\mathrm{fs}$, while keeping the temperature at $T = 300$ K with the help of a Nosé-Hoover thermostat. Prior to the production run we perform an additional 1 ns long NVT equilibration run at $T = 300$ K with $\Delta t = 1\,\mathrm{fs}$, in order to ensure that the system has relaxed to equilibrium.

Production runs correspond to fixed volume, number of particles and total energy of the system, using a velocity Verlet algorithm with timestep $\Delta t = 1\,\mathrm{fs}$. To induce a periodic change in the direction of the local dipolar moment of the C_{60}-X, CNT-X, and Y-CNT-X molecules we switch the value of the charge q from $q \to -q$ with a period τ.

Fitting procedure of dynamical parameters

As stated in the main text, the mean square displacement (MSD) of a spherical Brownian particle can be written in terms of three parameters: translational diffusion coefficient D_t, rotational diffusion coefficient D_r, and propelling speed v

$$\left\langle \Delta\vec{r}^2 \right\rangle = \left[6D_t + \frac{v^2}{D_r} \right] t + \frac{1}{2} \left(\frac{v}{D_r} \right)^2 \left[e^{-2D_r t} - 1 \right]. \tag{1}$$

This formula shows that three distinct regimes are to be expected: (a) for short times, but still larger than the molecular thermalization time scale, we get the usual diffusive behavior $\langle \Delta\vec{r}^2 \rangle = 6D_t t$; (b) for larger times, up to times of the order of $\tau_r \equiv D_r^{-1}$, superdiffusive (faster than linear) behaviour takes place, i.e. $\langle \Delta\vec{r}^2 \rangle = 6D_t t + 2v^2\tau_r t^2$; (c) for times larger than τ_r regular diffusive behavior is regained, $\langle \Delta\vec{r}^2 \rangle = (6D_t + v^2\tau_r/2)\, t$, an enhanced diffusion regime, i.e. a hot Brownian particle.

The three parameters (D_t, D_r, v) are obtained from the C_{60}-X simulations in a two step process. First, from the the angular MSD of the C-X direction (left panel in Fig. 3) we obtain D_r. The right panel in Fig. 3 displays the values obtained for $\tau_{rot} \equiv 1/D_r$ as a function of pulsating frequency (inverse of switching period).

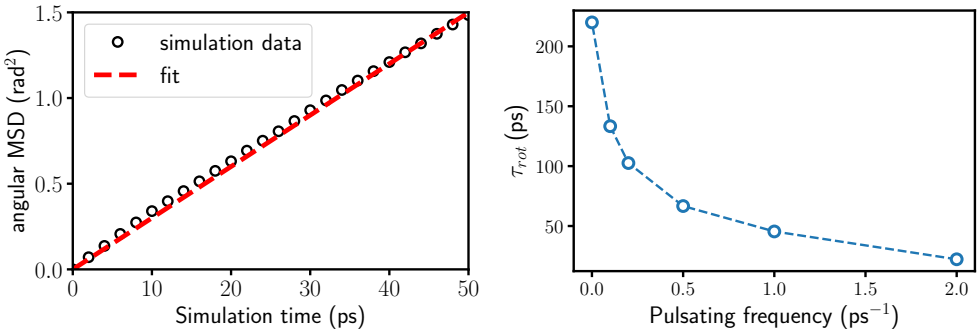

Figure 3: (Left) Angular mean square displacement of C_{60}-X with switching dipolar moment of $\tau = 10\,\text{ps}$; (Right) Rotational correlation time as a function of pulsating frequency.

Next, with the value of D_r in hand we observe that the center of mass MSD (Eq. 1) can

be alternatively written as

$$\left\langle \Delta\vec{r}^2 \right\rangle = D_t \cdot [6t] + v^2 \cdot \left[\frac{t}{D_r} + \frac{e^{-2D_r t} - 1}{2D_r} \right], \tag{2}$$

i.e. it is bilinear in the remaining free parameters D_t and v^2. We can thus extract them by a bilinear regression procedure. The left panel in Fig. 4 displays the center of mass MSD obtained from simulations and the fits produced by the regression procedure. The speeds that result are plotted in Fig. 2 of the main article, and the translational diffusion coefficients (D_t) can be found in the right panel of Fig. 4, as a function of pulsating frequency ($\equiv 1/\tau$).

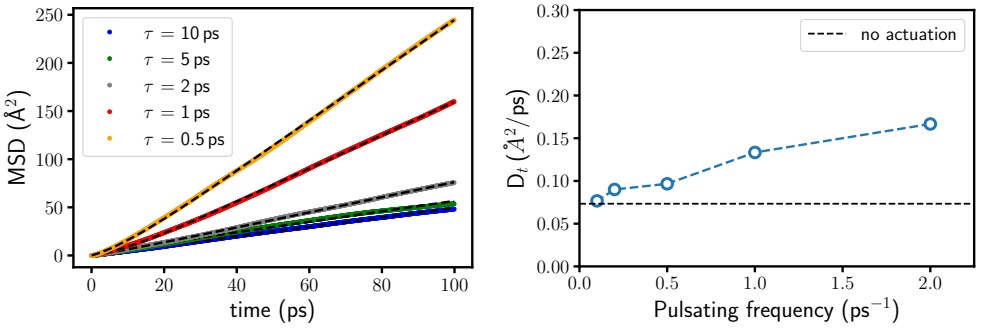

Figure 4: (Left) MSD of the C_{60}-X center of mass for different switching periods τ (dashed black lines represent the fit for each case obtained employing multiple regression); (Right) Dependence of the C_{60}-X diffusion coefficient on the pulsating frequency.

It is interesting to note that τ_r decreases with increasing power with respect to the free diffusion value, a feature also found for self-motile microscale swimmers[35]. Secondly, D_t increases with the power applied, although the effect is not so marked as for τ_r, both features also coincident with Ref. [35]. These features might thus be common at high power, and not due to numerical artifacts or imperfections of the swimmer.

Power absorbed

As a result of periodically switching the C_{60}-X dipole the solvent absorbs energy over time, which is reflected in an increase of the overall temperature of the system. This increase

depends on the period of dipole inversion, ranging from $\Delta T \approx 1\,\mathrm{K}$ for $\tau = 10\,\mathrm{ps}$ to $\Delta T \approx 50\,\mathrm{K}$ for $\tau = 0.5\,\mathrm{ps}$, in our typical 1ns-long simulations. Similar (although somewhat smaller) values for the temperature increase are obtained for simulations of the CNT-X molecule.

The power absorbed in this process can be easily calculated by monitoring the change in total energy of the system over the time during which the C_{60}-X (or the CNT-X) molecules are actuated. In Fig. 5 we show the power absorbed by the system as a function of the pulsating frequency of dipole switching, both for the C_{60}-X and CNT-X molecules. As expected, in both cases the power deposited into the system linearly increases with the frequency of actuation on the C-X dipole. Note that the efficiency of energy absorption is slightly larger for the C_{60}-X case, what we attribute to the fact that the dipole is surrounded by a larger number of water molecules, in comparison to the CNT-X case for which, due to the confining nanotube, the number of surrounding water molecules is limited.

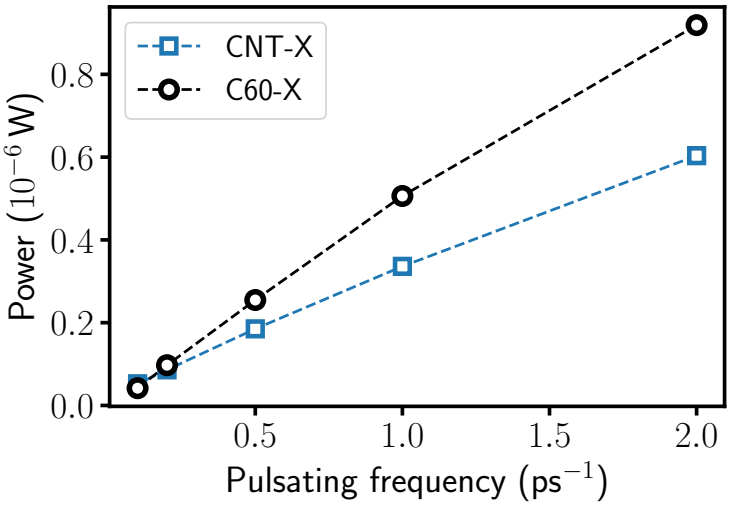

Figure 5: Power absorbed as a function of the dipole pulsating frequency for the C_{60}-X molecule in bulk water, and for the CNT-X molecule confined in a hydrated nanotube.

Photobleaching

It is well known that cycling ultimately leads to photobleaching of the fluorophore. To assess its possible impact on the propulsion mechanism, it is important to compare the number of cycles required for degradation with that required for our mechanism to result in measurable propulsion. As for photostability, there is a large range depending on the fluorophore (from 700 cycles to 3 million, Table 23.1 of Ref. [40] of main text), with good fluorophores reaching up to 10^5 to 10^6 cycles prior to degradation. This number can be compared with the number of cycles in our simulations: taking the average case (inversion period $\tau = 2$ ps), a strong thermophoretic effect (with speed larger than 1 m/s) is observed during simulations of the order of 1 ns, i.e. only 500 cycles are completed (less than for the most labile fluorophore). In order to better assess whether enhanced mobility would be measurable, we start referring to our estimation of power involving Cu153, from which we inferred a speed in excess of 0.1 m/s for switching characterized by $\tau = 10$ ps. In typical Fluorescence Correlation Spectroscopy experiments, a standard technique, the characteristic length of the observational volume is ~ 1 μm, which would be traversed in ~ 0.1 μs (assuming a confined geometry for the swimmer). This would require $\sim 10^4$ switches, significantly below the number of cycles before degradation in good fluorophores. It should be added that this number, although computed for a high power, may actually be independent of the switching rate for a fixed distance, if we adopt the reasonable assumption that the linear relation between speed and power holds for decreasing powers. We start by noting that $v = \alpha \cdot P$ (Eq. 2 of main text), and that the power deposited is proportional to switching frequency (see Fig. 5 in SI), $P = \beta \cdot f = \beta/\tau$. We therefore have $v = \alpha \cdot \beta/\tau$, with α and β being constants. For a fixed distance L this results in a time of transit $t = L/v = L \cdot \tau/\alpha \cdot \beta$, so that $t/\tau =$ number of switches = constant independent of power. It seems therefore feasible to observe the swimmer entering and exiting the observational volume before degradation, and without requiring high power sources.

Propulsion speed vs. swimmer dimensions

Our results show similar values for the propulsion speed of the C_{60}-X molecule in bulk and the CNT-X in confinement. Due to their different size, for the same actuation mechanism and solvent one would expect the CNT-X to exhibit a larger drag coefficient and consequently lower speeds. This can be seen more precisely approximating the CNT-X molecule to a long cylinder and using slender body theory[6] to estimate the drag coefficient. Considering that the motion of the CNT-X molecule occurs in the direction of its axis, the drag coefficient is given by[6]

$$\xi_{CNT-X} = \frac{2\pi\eta L}{\log(L/a) - 1/2} \tag{3}$$

where L and a are the length and the radius of the rod, and η is the viscosity of the solvent. On the other hand, the drag coefficient of the C_{60}-X molecule is approximately given by the Stokes formula

$$\xi_{C60-X} = 6\pi\eta R\,, \tag{4}$$

with R being the radius of the spherical particle. If the viscosity of the solvent is the same $\xi_{CNT-X}/\xi_{C60-X} \approx 1.65$.

In our case, although for both molecules the solvent is the same, the CNT-X molecule propels in a strongly confined region, the interior of a (20,20)-CNT (with a diameter of ≈ 2.5nm). In such strong confinement, it is known that the rheological properties of water are significantly affected, with a reduction of its effective viscosity. This is shown in Fig. 4 of Ref. [47], where the effective viscosity of water confined in the interior of a CNT is shown as a function of the CNT's diameter. For a diameter of ≈ 2.5nm a reduction of the effective viscosity of water with respect to bulk is obtained, by a factor ≈ 0.68 ($\eta = 0.7$mPa·s under such confinement and $\eta = 1.02$mPa·s for bulk water). Consequently, if we take into account the difference in viscosities due to confinement we obtain

$$\frac{\xi^{confinement}_{CNT-X}}{\xi^{bulk}_{C60-X}} \approx 1\,. \tag{5}$$

This is consistent with the results obtained for the speed as a function of input power reported in the article.

References

(1) Robinson, M.; Suarez-Martinez, I.; Marks, N. Generalized Method for Constructing the Atomic Coordinates of Nanotube Caps. *Phys. Rev. B* **2013**, *87*, 155430.

(2) Robinson, M.; Marks, N.; NanoCap: A Framework for Generating Capped Carbon Nanotubes and Fullerenes. *Comput. Phys. Commun.* **2014**,*185*, 2519.

(3) Humphrey, W.; Dalke, A.; Schulten, K. VMD – Visual Molecular Dynamics. *J. Mol. Graph.* **1996**, *14*, 33.

(4) Plimpton, S. Fast Parallel Algorithms for Short-Range Molecular Dynamics. *J. Comput. Phys.* **1995**, *117*, 1.

(5) Price, D. L.; Brooks III, C.L. A Modified TIP3P Water Potential for Simulation with Ewald Summation. *J. Chem. Phys.* **2004**, *121*, 10096.

(6) C. Duprat, C. and Shore, H.H. *Fluid-Structure Interactions in Low-Reynolds-Number Flows*, Royal Society of Chemistry, 2015.